

Flow Control And Thermal Management Using Dielectric Glow Discharge Concepts

Balaji Jayaraman¹ and Wei Shyy²

Department of Mechanical and Aerospace Engineering
University of Florida, Gainesville, FL 32611, USA

Abstract

The glow discharge creates a thermal plasma far from thermodynamic equilibrium, and can be fruitfully employed for active flow control and thermal management. In the present study, we investigate a capacitively coupled radio frequency discharge plasma generator, where the plasma is generated on the surface of a dielectric circuit board with electrode strips on the top and bottom. A recently developed phenomenological modeling approach is employed to probe force generation as well as aerodynamics and heat transfer characteristics. Qualitative and quantitative evaluations are made based on available experimental measurements to highlight the performance of this device concept and physical implications. Consistent and noticeable increases in lift, drag and heat transfer rates are observed while varying the Reynolds number and angle of attack, indicating that there is substantial potential of applying this concept to manage and control fluid flow and thermal environments.

Nomenclature

a	Plasma breakdown length perpendicular to the surface
b	Plasma breakdown length along the surface
C_p	Specific heat
C_L	Lift coefficient= $L/(\rho U^2/2)$
d	Gap between electrodes
D	Drag force
e	Internal energy
e_c	Electron charge
E	Electric field strength
E_0	Peak electric field strength
E_b	Breakdown field strength
F	Force from glow discharge plasma
H	Heat transfer
k_1, k_2	Electric field gradients
K	Coefficient of thermal conductivity
l	Length of the plate
L	Lift force
Nu	Nusselt number= $HL/K(T_p-T_a)$
p	Pressure
Pr	Prandtl number= $C_p\mu/K$

Re	Reynolds number= $\rho ul/\mu$
T	Time period of voltage cycle
T_a	Ambient fluid temperature
T_p	Temperature of the plate
U	Inlet fluid velocity
V	Applied voltage
x,y	Coordinate axes
ρ	Fluid Density
ρ_c	Charge number density
μ	Viscosity
τ	Shear stress
Δt	Discharge duration per unit cycle
ϵ_0	Permittivity of free space= 8.852×10^{-12} Farad/m

1. Introduction

Glow discharge operates in a highly non-equilibrium plasma regime with little thermal effect while exhibiting substantial fluid dynamics characteristics. It offers interesting potential for active fluid flow and thermal control¹⁻⁷. As schematically illustrated in Fig. 1, the plasma generation is achieved using a capacitively coupled mechanism on the surface of a dielectric board containing asymmetrically distributed electrodes on the top and bottom. For example, Corke et al²⁻³ demonstrate that the plasma operation enhances lift and also causes an increase in drag ascribed to flow separation downstream of the plasma generating electrode.

Physically, the plasma generation produces a wall jet on the surface, essentially acting as a source of external momentum to the fluid. This force is termed paraelectric by Roth et al⁴. In order to develop an analysis framework to probe the physics and engineering implications, a computational model based on simplified electromagnetic field description and the Navier-Stokes equations has been developed by Shyy et al¹. The paraelectric force is modeled as a body force term in the Navier-Stokes equations governing the fluid flow. The underlying principle behind this treatment is that the paraelectric force can be viewed as that exerted on the local charge concentration of the plasma by the local electric field. This force acts on the fluid inside the elemental volume of interest. This modeling approach is reasonable in light of the plasma being weakly ionized and hence the force on the charge particles is equivalent to the force acting on the fluid itself. Based on such a

¹ Graduate Student Assistant

² Professor and Dept. Chair, Fellow AIAA

Copyright © 2003 by Authors, published by American Institute of Aeronautics and Astronautics, Inc. with permission.

notion, if we consider the local electric field as $E(x,y)$ and the local charge number density as $\rho_c(x,y)$ then, the net force acting on the fluid particle locally is given by

$$\vec{F} = \vec{E}(x, y)\rho_c e_c \quad (1)$$

The relationship between the charge and the electric field strength is given by Maxwell's equations as

$$\vec{\nabla} \cdot \vec{E} = \frac{\rho_c e_c}{\epsilon_0} \quad (2)$$

Coupling the two we get the expression for the force as

$$\vec{F} = \epsilon_0 \vec{E} \left(\vec{\nabla} \cdot \vec{E} \right) \quad (3a)$$

or

$$\vec{F} = \vec{\nabla} \left(\frac{1}{2} \epsilon_0 E^2 \right) \quad (3b)$$

The above expression in Eq. (3b) is the force per unit volume as presented by Roth et al⁴. Shyy et al¹ have independently adopted a conceptually similar approach by taking advantage of the geometry of the plasma generation device shown in Fig. 1 to simplify the electric field computations. The strip used in the experiment by Mclaughlin et al⁶ shown in Fig. 1b, is less than a millimeter in thickness and creates nearly two-dimensional flows. A schematic illustration of the field lines presented in Fig. 2 indicates high degrees of concentration at the upper electrode and an almost uniform distribution on the lower electrode surface. With the electrode being thin, it is reasonable to linearize the field variation in space without solving the detailed Maxwell equation, thus substantially simplifying the computational task. Specifically, the field lines here are such that the strength of the field decreases as one moves far away from the electrodes. This variation of E can be written as

$$|\vec{E}| = E_0 - k_1 x - k_2 y \quad (4)$$

where E_0 is the maximum electric field in the region of plasma operation and k_1 and k_2 being strictly positive. E_0 can be approximated as

$$E_0 = \frac{V}{d}, \quad (5)$$

where d is the separation between the two electrodes in the x direction (Fig. 1). The constants k_1 and k_2 are evaluated by using the condition that the field strength is the breakdown value at the plasma-neutral fluid boundary. Hence we can directly compute k_1 and k_2 as

$$k_1 = \frac{E_0 - E_b}{b} \quad (6a)$$

and

$$k_2 = \frac{E_0 - E_b}{a} \quad (6b)$$

The components of the electric field are given by

$$E_x = \frac{Ek_2}{\sqrt{k_1^2 + k_2^2}}, \quad (7a)$$

$$E_y = \frac{Ek_1}{\sqrt{k_1^2 + k_2^2}}. \quad (7b)$$

The above expressions represent only the instantaneous values as the field strength fluctuates in time. However, the high frequency of the applied voltage (a few KHz) and the substantially slower fluid flow time scales makes it reasonable to model the glow discharge effect as a time invariant phenomenon. Nevertheless, the glow discharge plasma is not generated throughout the whole cycle of the voltage. In order to address this issue, Shyy et al¹ introduce a duty cycle factor which is equivalent to time averaging the force. The body force components along the x and y directions, f_x and f_y , based on the local electric field and charge density are

$$f_x = E_x \rho_c e_c, \quad (8a)$$

$$f_y = E_y \rho_c e_c. \quad (8b)$$

If we include the duty cycle factor, then the net force expressions are

$$F_x = \frac{f_x \Delta t}{T}, \quad (9a)$$

$$F_y = \frac{f_y \Delta t}{T}. \quad (9b)$$

The resulting model is represented as the local body force per unit volume, which can be substituted into the Navier-Stokes equations. No attempt is made to establish a criterion for the plasma formation, which requires extensive analysis of plasma dynamics.

Enloe et al⁵ present a detailed experimental study to determine the mechanism of the plasma actuator. The study suggests the presence of a characteristic temporal and spatial structure, and the plasma as a dielectric barrier discharge (DBD). These DBD's have been extensively studied before and their properties have been well documented⁸⁻¹². More importantly, the study discounts bulk heating of the fluid or discharge asymmetry as reasons behind the plasma-fluid coupling.

The temporal structure of the DBD plasma indicates noticeably different discharge patterns in the two half cycles. The discharge is consistently regular and continuous when the exposed electrode is more negative and irregular otherwise. Further a continuously increasing voltage is necessary to sustain the discharge and the intensity heavily depends on the rate of increase. It is apparent that the difference in the two half cycles is the discharge duty cycle.

The present model takes advantage of this disparity in the plasma operation times and considers only the efficient half cycle for calculations. Enloe et al⁵, study the role of this discharge asymmetry by using a positive and negative saw tooth input voltage waveform

and compare the thrust generated. The outcome is that the positive saw tooth produces more thrust for the same power consumption. The saw tooth waveform is asymmetric in time. In the case of positive saw tooth waveform, the voltage polarity with the higher operation time is more efficient with a regular discharge while for the negative saw tooth, the discharge is irregular for a majority of the cycle. The present model can clearly reproduce this qualitative behavior with the duty cycle of plasma formation being a critical input parameter along with the peak voltage.

The above study clearly indicates that the disparity in plasma strengths for opposite voltage polarities causes the difference in thrust. It was argued in the present model¹, that the direction of the induced flow is caused by this discharge asymmetry with the effect of the weaker half cycle being suppressed. In fact, the discharge asymmetry in that case was reasoned¹ based on the electrode geometry. However in an experimental study where both the electrodes were encapsulated, but the geometric asymmetry maintained, there was still a weak induced flow being generated. This indicates that the geometric asymmetry in fact plays a role in the direction of the resultant flow. However, the exact nature of the effect of geometry on the induced flow direction is not clearly evident and requires further insight. A time-dependent simulation taking into account Debye shielding effects will augment the understanding of the spatial plasma structure which is required to gauge the role of the geometric asymmetry.

In the present study, we have made detailed computations, in consultation with the available experimental evidence to estimate the force generation as well as the fluid flow and heat transfer characteristics generated by plasma. After summarizing the computational model, first, a detailed force evaluation exercise is carried out to assess its accuracy. Next, the model is employed to investigate the aerodynamics and heat transfer for flow control over a flat plate under different Reynolds numbers and angles of attack.

2. Governing Equations

The computational model consists of the Navier-Stokes equations and the energy transport equation for a steady, incompressible flow. The body force terms, which are added to the momentum equations, reflect the effect of the glow discharge on fluid flow. The fluid is assumed to be incompressible in view of the plasma being essentially isothermal. The electric field along the straight line (Fig. 2) from (0,0) to (d, 0) is E_0 . Similarly, the electric field on the straight line joining (0,a) and (b, 0) has a value E_b . In the following, we offer a complete set of governing equations, in the two-dimensional form

$$\frac{\partial \bar{A}}{\partial t} + \frac{\partial \bar{B}}{\partial x} + \frac{\partial \bar{C}}{\partial y} = \bar{D}, \quad (10a)$$

$$\bar{A} = \begin{bmatrix} \rho \\ \rho u \\ \rho v \\ e \end{bmatrix}, \quad (10b)$$

$$\bar{B} = \begin{bmatrix} \rho u \\ \rho u^2 + p - \tau_{xx} \\ \rho uv - \tau_{xy} \\ u(e+p) - \tau_{xx}u - \tau_{xy}v - k\partial_x T \end{bmatrix}, \quad (10c)$$

$$\bar{C} = \begin{bmatrix} \rho v \\ \rho uv - \tau_{xy} \\ \rho v^2 + p - \tau_{yy} \\ u(e+p) - \tau_{xy}u - \tau_{yy}v - k\partial_y T \end{bmatrix}, \quad (10d)$$

$$\bar{D} = \begin{bmatrix} 0 \\ F_x \\ F_y \\ 0 \end{bmatrix}, \quad (10e)$$

where τ_{xy} is the shear stress. The F_x and F_y , body force terms given from Eq. (9) have a value of zero in a region where we do not have the plasma.

2.1. Boundary conditions

The no-slip condition when applied at the solid wall yields,

$$u = v = 0. \quad (11)$$

At the outlet, zero velocity gradient is assigned taking advantage of the negligible influence of the plasma, far away from the electrode. At the inlet, the fluid enters with a uniform velocity U and the ambient temperature T_a . The plasma discharge boundary is specified by

$$\rho_c = 0 \text{ for } E < E_b. \quad (12)$$

3. Results and discussion

3.1. Force evaluation

The aforementioned computational model¹ representing the effect of the plasma as a local force distribution is simple to implement. The main focus of the present study is to assess the accuracy of the model. A particular issue pertaining to the model is the procedure for employing the experimental data to fix up the parameters such as the duty cycle. In the following, we present the force prediction under the quiescent condition, in accordance with the experiment conducted by Mclaughlin et al⁶. In these experiments, the force

measured is the shear caused by the induced flow on the contact surface in a quiescent environment. After incorporating the duty cycle factor, the force acting on a fluid element from Eqs. (7) and (8) is

$$F_x = \frac{\Delta t}{T} \rho_c e_c E_x A dx \quad (13)$$

where A is the area of the face of the differential volume perpendicular to the orientation of dx and E_x is the component of the electric field in the x-direction. Under the linear field approximation, the net force in the x-direction, F_x , acting on the contact surface is

$$F_x = \int_0^b E n_x \frac{\Delta t}{T} \rho_c e_c A dx = \int_0^b \frac{\Delta t}{T} (E_0 - k_1 x) n_x \rho_c e_c A dx, \quad (14)$$

where n_x is the direction cosine, b is the plasma breakdown distance, illustrated in Fig. 2b. Here, k_2 is neglected as $y=0$ on the surface. From the Maxwell equation, Eq. (2), we get

$$\left| \frac{dE}{dx} \right| = |k_1| = \left| \frac{\rho_c e_c}{\epsilon_0} \right| \quad (15a)$$

The absolute values are taken so that we can conveniently ignore the sign conventions while defining the charge on an electron. Substituting for k_1 from Eq. (6a) into Eq. (15a), we get

$$\rho_c b = \epsilon_0 \frac{(E_0 - E_b)}{e_c} \quad (15b)$$

The above equation (15a) when substituted in the expression for the force in Eq. (14) gives,

$$F_x = \int_0^b \frac{\Delta t}{T} (E_0 - k_1 x) n_x k_1 \epsilon_0 A dx. \quad (16a)$$

Substituting for k_1 and evaluating the integral we get

$$F_x = \left(\frac{E_0^2 - E_b^2}{2} \right) \epsilon_0 n_x A \frac{\Delta t}{T}. \quad (16b)$$

Note that, by assuming the linear variation for E, we are fixing the direction cosine n_x from the choice of the breakdown lengths a and b.

These two equations (15b) and (16b) relate the three parameters, namely E_0, ρ_c and b with the force. The duty cycle also varies with the voltage but is assumed constant in the present discussion. All other parameters in the expression for the force in Eq. (16b) are fixed within the modeling framework. For a start, let us assume the knowledge of the force F and the plasma breakdown length b for a particular value of the voltage. This helps us to calculate the charge number density ρ_c from Eqs. (15) & (16). In order to extend the knowledge of two parameters, ρ_c and b, we assume a linear proportionality for above parameters with the applied voltage. The experimental results by Mclaughlin et al⁶ present the force generated for various voltages with an electrode 0.625mm wide and Teflon dielectric. Lets us start with a voltage $V=4.66KV$, for which, from the

direct measurement, $F=0.3969mN$ and from light intensity measurements given in [6], one deduces that $b=2.8$ mm for the present electrode configuration. The various parameters that are assumed invariant in the present framework are

$$\frac{\Delta t}{T} = 0.77$$

$$\epsilon_0 = 8.852 \times 10^{-12} \text{ Farad / m}$$

$$A = 1.15 \times 10^{-6} m^2$$

$$n_x = 0.89$$

The above duty cycle for a sine waveform of the applied voltage has been deduced experimentally by Mclaughlin et al⁶. By substituting the above data into Eq. (15), we get $\rho_c = 1.59 \times 10^{11}/cm^3$. Now, the charge number density and the length b are fixed for the assumed voltage. The values of the same for any other voltage can be scaled as:

$$\frac{\rho_{c1}}{\rho_{c2}} = \frac{V_1}{V_2} \quad \text{and} \quad \frac{b_1}{b_2} = \frac{V_1}{V_2}. \quad (17)$$

These values can be substituted back into Eqs. (15b) and (16b) to obtain the force. The comparison between the experimentally recorded force and the calculated force is presented in Fig. 3. Here the F_{actual} represents experimentally measured force while the $F_{\text{calculated}}$ represents the predicted values. While there is a quantitative deviation between the experimental and computational values, the trends between them are consistent. The different results likely arise from linearization of the electric field as well as simplification made during the scaling process described above. Based on this exercise, we now employ the present computational model to explore the potential of flow control and thermal management.

3.2. Effect of plasma on aerodynamics

The computational model consists of a flat plate placed in a free stream of fluid as shown in the Fig. 4. The electrode arrangement serving as an actuator is placed at the middle of the plate. The computational domain encloses the flat plate and electrode arrangement. The boundary conditions for the domain are as shown in Fig 4. To reduce the computational domain and to attain the desirable accuracy, the plate is chosen to be 1cm long, so that the electrode, 0.5mm long and 0.25mm thick, can be adequately modeled without excessive computational resources. The main interest here is to probe the effect of the glow discharge-induced fluid flow on the existing flow structures, for both attached and separated fluid flows. The number of grid points used for the simulation is 161x102. The grid distribution is focused towards capturing the modified flow field in the vicinity of the plasma. The grid points are more clustered near the plate and near the leading edge. The numerical simulation employs a multiblock model solved by a second-order upwind scheme. Detailed discussions can be found in

Shyy et al¹³⁻¹⁴. It is to be noted that, wherever not mentioned, the values for the voltage, frequency and Re are 4KV (rms), 3KHz and 333 respectively. The values of the free stream velocity are 0.2,0.4 and 0.5m/s, and for air, resulting in the Reynolds numbers of 133,266 and 333, based on the plate length, of 0.01m.

(i) Fluid Flow

The effect of the plasma on various flows at different Reynolds numbers and angles of attack are studied. The drag is calculated based on the loss of momentum flux in the free stream direction. In the presence of the plasma, the momentum loss will include the glow discharge-induced body force effect. Figure 5 presents the variation of the drag coefficient with angle of attack for a given Reynolds number in the presence of the plasma. Irrespective of Re, the plasma induced additional drag, which corroborates with the results reported by Corke et al²⁻³. More importantly, the magnitude of increase in the drag coefficient C_D appears insensitive to angles of attack for a particular Re for the two lower angles of attack (0 and 8 degrees) when the flow structure is the same, i.e., attached. For a 20-degree angle of attack where the flow separates, the plasma modifies the flow structure, resulting in a different drag level. Also, the increase in drag coefficient becomes smaller as Re increases. This decrease in effect of the plasma for higher Re has been explicitly pointed out by Shyy et al¹. The body force term used in the momentum equation is independent of Re and hence becomes smaller when normalized by the dynamic head. By considering the increase in drag force ΔD defined by

$$\Delta D = \Delta C_D \times \frac{1}{2} \rho U^2, \quad (18)$$

instead of the drag coefficient, for a given angle of attack. It is observed from Table 2 that the drag force is largely independent of the Reynolds number in the absence of flow separation. Similar trends are observed in the experimental results presented by Corke et al²⁻³. Figure 7a illustrates the effect of varying voltage on the drag while other parameters are maintained constant. The drag increases linearly with voltage in the absence of flow separation.

Figure 6 presents the variation of lift coefficient with Re for a given angle of attack. In general, the plasma on case yields a higher lift. In Fig. 6 and Table 3, the increase in lift coefficient becomes smaller as Re increases. However, for separated flows as shown in Fig. 6b, there are more substantial increases in lift compared to the attached flow (Fig. 6a) with the same glow discharge parameters and Re. As indicated in Table 3, and consistent with the drag force, as Re becomes sufficiently high, the increase in lift force appears to stabilize. Figure 7b presents the lift variation with voltage for the case with flow separation. The non-

linearity is due to the separation region changing with the magnitude of the body force.

(ii) Heat Transfer

The heat transfer enhancement resulting from glow discharge has been briefly discussed by Shyy et al¹. In the present study the heat transfer is studied for various Re and angles of attack. Figure 8 presents the Nusselt number variation with the angle of attack for various Re. The Nusselt number here is given by

$$Nu = \frac{Hl}{K\Delta T}, \quad (19)$$

where H is the heat flux, l is the characteristic length of the plate, K is the coefficient of thermal conductivity and ΔT is the temperature difference between the ambient fluid and the hot surface, which is set to a non-dimensional value of unity. In all cases, the heat transfer is enhanced during plasma operation and especially so when the angle of attack is high and flow separates. Moreover, the glow discharge-enhanced Nusselt number only exhibits modest variations versus the angle of attack.

The plasma helps reattach the flow and enhances heat transfer. The modest deviation in Nu for the high angle of attack cases is due to the incomplete removal of the re-circulation zone. One way to further improve the heat transfer rate is to place multiple electrodes along the stream wise direction to induce stronger fluid flows and also eliminate the re-circulation zone. In Fig.9, the variation of heat transfer rate with the applied voltage is presented with the Nu stabilizing after a few kilovolts, although their paths are different for attached and separated flows.

(iii) Effect of electrode position on the flow

To investigate the effect of the electrode placement position on the flow, two positions (middle of the plate and at a distance of 10 percent length (of the plate) from the leading edge) were considered. The study was conducted for an angle of attack of 20-degrees and Re=333. Shown in Table 4 is a comparison of the aerodynamic and heat transfer data.

It appears that the effect of the electrode position on the drag is insignificant. As summarized in Table 4, there are only minor changes in aerodynamics and heat transfer coefficients. Figure 10 compares the streamlines of the flow over a flat plate, with Re=333 and an angle of attack of 20 degrees. Figure 10a representing the no plasma case shows a large flow separation. In Fig. 10b the electrode is placed at the middle of the plate, while in Fig. 10c, the electrode is closer to the leading edge. While the forwardly placed electrode can more effectively eliminate the flow separation, both electrode locations produce very comparable outcome in aerodynamics and heat transfer. It seems that the overall impact of the glow discharge,

namely, the induced wall jet is not sensitive to the details of the local flow structures for the Re considered, making the present device very attractive for active control. Similar, experimental observations have also been reported by Corke et al²⁻³. In fact Corke et al, report efficient separation control at angle of attacks well past the stall angle. Also a typical plasma actuator with capacities described above leads to substantial pressure recovery and also manifold increase in the lift to drag ratio.

4. Summary and conclusions

A computational procedure for modeling and predicting glow-discharge induced flows is presented. To establish the model parameters, one requires knowledge of the plasma operation information such as the breakdown length and measured force for one specific voltage. Overall, the model can capture the overall trend between the force generation and the device operation. This body force modeling when used to study the aerodynamics and heat transfer past a flat plate, yielded qualitative agreement with the experimental work of Corke et al². Specifically, both lift and drag on the plate increase in the presence of the plasma. The impact on separating flows is more substantial because the flow tends to reattach. For heat transfer, the Nusselt number increases for the plasma on case, but the increase is insensitive to angle of attack for the present strength of the plasma considered. In all glow discharge induced flows promise fruitful opportunities for flow control and thermal management in various flow and thermal environments.

Acknowledgment

The present study has been supported in part by the US Air Force and TRW Foundation.

References

1. W.Shyy, B.Jayaraman and A.Andersson, Modeling of glow discharge-induced fluid dynamics, *J. App. Phys.*, Vol.92, no. 11, 6434-6443, December 1, 2002
2. T.C. Corke, E.J. Jumper, M.L. Post, D. Orlov and T.E. McLaughlin, Application of weakly ionized plasmas as wing flow-control devices, *AIAA 40th Aerospace Sciences Meeting & Exhibit*, Reno, NV (2002).
3. M.Post and T.C Corke, Separation control on high angle of attack airfoil using plasma actuators, *AIAA paper 2003-1024 41st Aerospace sciences meeting & Exhibit*, Reno, NV (2003).
4. J.R. Roth, D.M. Sherman and S.P Wilkinson, Boundary layer flow control with a one atmosphere uniform glow discharge surface plasma, *AIAA 36th Aerospace Sciences Meeting & Exhibit*, Reno, NV (1998).
5. C.L.Enloe, T.E.McLaughlin, R.D. Van Dyken, K.D.Kachner, E.J.Jumper and T.C.Corke, Mechanisms and responses of a single dielectric barrier plasma, *AIAA Paper 2003-1021 41st Aerospace sciences meeting & Exhibit*, Reno, NV (2003).
6. T.McLaughlin, private communication, US Air Force Academy, 2002.
7. F. Massines, A. Rabehi, P. Decomps, R.B. Gadri, P. Ségur and C. Mayoux, Experimental and theoretical study of a glow discharge at atmospheric pressure controlled by dielectric barrier, *J. Appl. Phys.* **83**, 6 (1998).
8. J. Li and S.K Dhali, Simulation of microdischarges in a dielectric-barrier discharge, *J.Appl.Phys.* **82**, 9 (1997).
9. V.I Gibalov and G.J Pietsch, The development of dielectric barrier discharges in gas gaps and on surfaces, *J.Phys. D:Appl. Phys.* **33**, 2618-2636, (2000).
10. S.Liu and M. Neiger, Excitation of dielectric barrier discharges by unipolar submicrosecond square pulses, *J. Phys. D: Appl. Phys.* **34**, 1632-1638, (2001).
11. W.S.Kang, Y.Kim and S.H.Hong, Spatio-temporal images of single streamer propagation in dielectric barrier discharge, *IEEE transactions on plasma science*, **30,1**, 166-167, (2002).
12. Z.Falkenstein and J.J.Coogan, Microdischarge behaviour in the silent discharge of nitrogen-oxygen and water-air mixtures, *J.Phys. D:Appl. Phys.* **30**,
13. W. Shyy, S. Thakur, H. Ouyang, J. Liu and E. Blosch, *Computational Techniques for Complex Transport Phenomena* (Cambridge University Press, New York, 1997).
14. W. Shyy, *Computational Modeling for Fluid Flow and Interfacial Transport* (Elsevier, Amsterdam, Netherlands, 1994).
15. S. Hippler, M. Pfau, K.H. Schmidt and Schoenbach (Eds.), *Low Temperature Plasma Physics: Fundamental Aspects and Applications*, 15+331-339 (Wiley-VCH, Berlin, 2001). 817-825, (1997).
16. J.List, A.R Byerly, T.E McLaughlin, R.D Van Dyken, Using a plasma actuator to control laminar separation on a linear cascade turbine blade, *AIAA Paper 2003-1026 41st Aerospace sciences meeting & Exhibit*, Reno, NV (2003).
17. B.Pashaie, S.K Dhali, F.I Honea, Electrical characteristics of a coaxial dielectric barrier discharge, *J. Phys. D: Appl. Phys.* **27**, 2107-2110 (1994).
18. J.R Roth, H.Sin, R.C.M Madhan and S.P Wilkinson, Flow re-attachment and acceleration by paraelectric and peristaltic electrohydrodynamic effects, *AIAA Paper 2003-0531 41st Aerospace sciences meeting & Exhibit*, Reno, NV (2003).

Peak voltage	Measured force(mN)
3.56	0.118
4.66	0.397
5.76	1.03
7.34	2.43

Table 1. Force measured experimentally by Mclaughlin et al for different input voltages (sine waveform) at 3KHz frequency.

Re	133	266	333
ΔC_D	2.8	0.71	0.46
$\Delta D(N) = \frac{1}{2} \rho U^2 \times \Delta C_D$	6.72	6.816	6.9

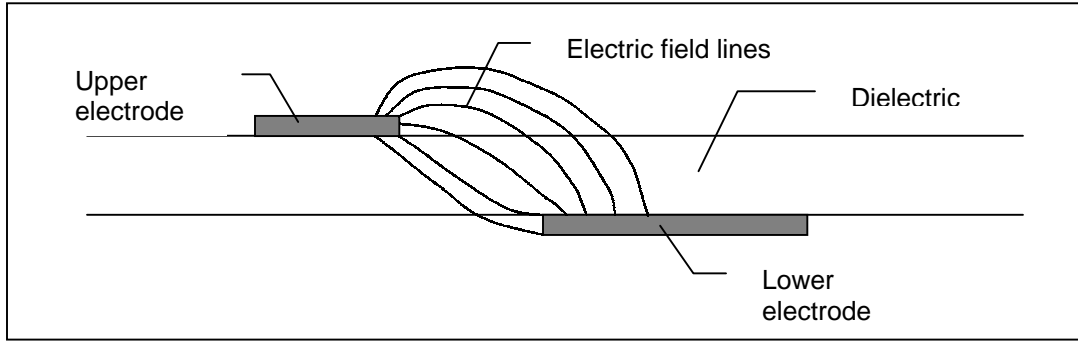
Table 2. Change in drag coefficient and drag force with Reynolds number.

Re(AoA=8)	133	266	333
ΔC_l	1.51	0.435	0.297
$\Delta L(N) = \frac{1}{2} \rho u^2 \times \Delta C_l$	3.624	4.176	4.455

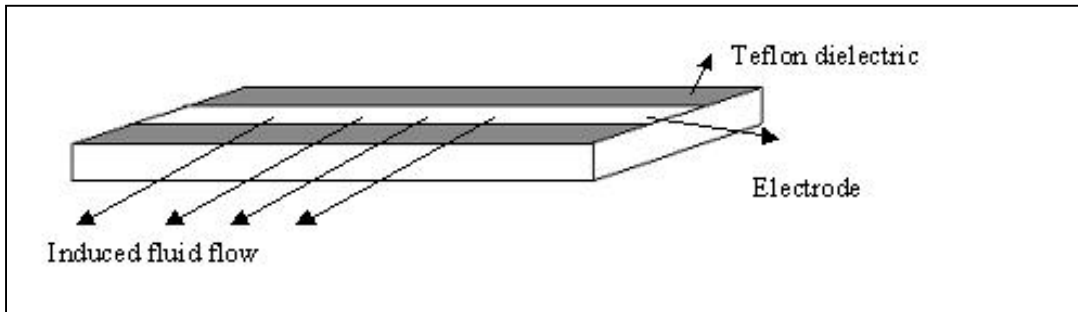
Table 3. Change in lift coefficient and lift force with Reynolds number.

Electrode position	middle	10% from leading edge	No plasma
Aerodynamic data			
Drag coefficient	1.0	1.0	0.124
Lift coefficient	1.22	1.12	0.636
Nusselt number	28.35	29.57	18.04

Table 4. Effect of electrode position on aerodynamic and heat transfer properties.

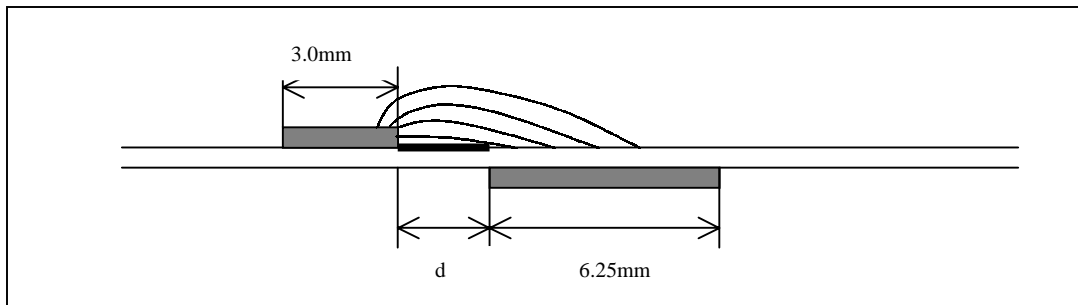


(a) Arched electric field lines due to asymmetric configuration of electrodes.

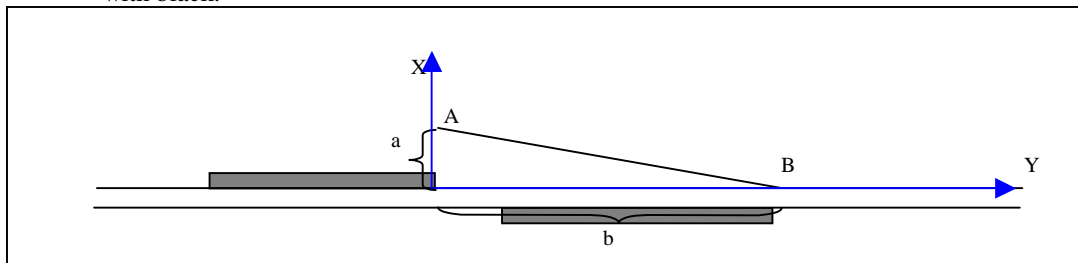


b) Model of the actuator used by Mclaughlin et al with the strip electrode and Teflon dielectric

Figure 1. Schematic representation of electrode geometry along with the field lines and the various glows associated with it during plasma formation. Note the concentration of field lines at the upper electrode and an even distribution on the dielectric.



(a). Rough shape of electric field lines. The region with the strongest electric field, E_0 , is filled with black.



(b) The line A-B constitutes the plasma boundary using linear approximation. The electric field strength outside this line is not strong enough to ionize the air.

Figure 2. Schematic of electrode geometry and electric field lines indicating linear approximation.

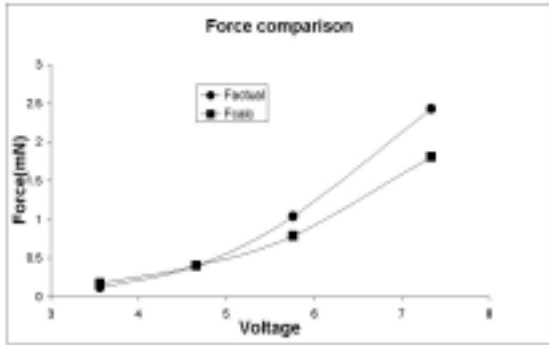


Figure 3. Comparison of the experimental and calculated plasma force for different voltages.

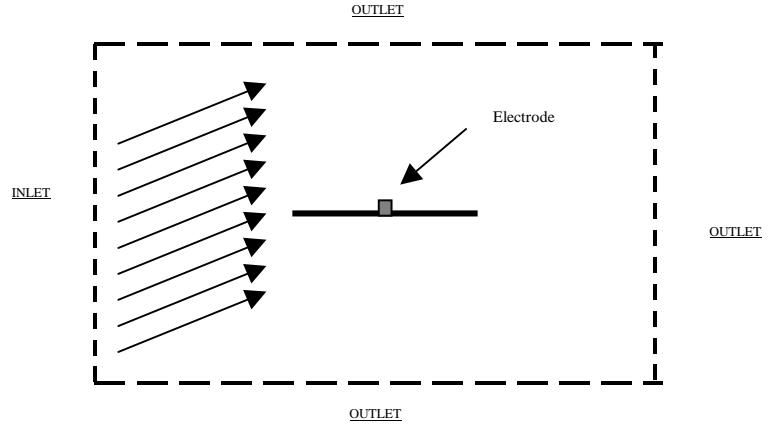
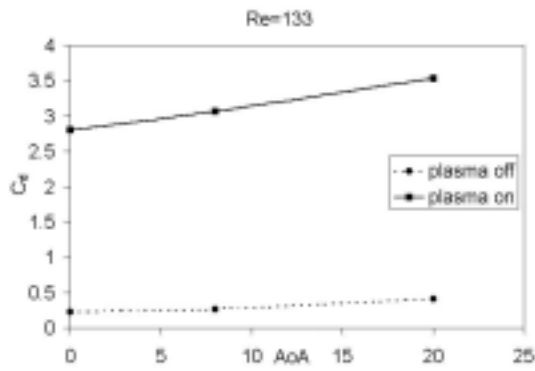
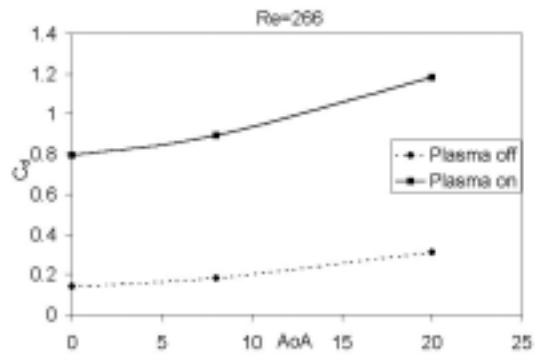


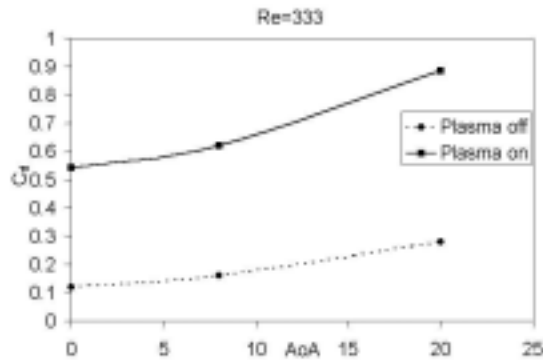
Figure 4. A schematic of the computational domain with the flat plate and the electrode. The electrode in fact has negligible thickness in the above arrangement.



(a) Re=133

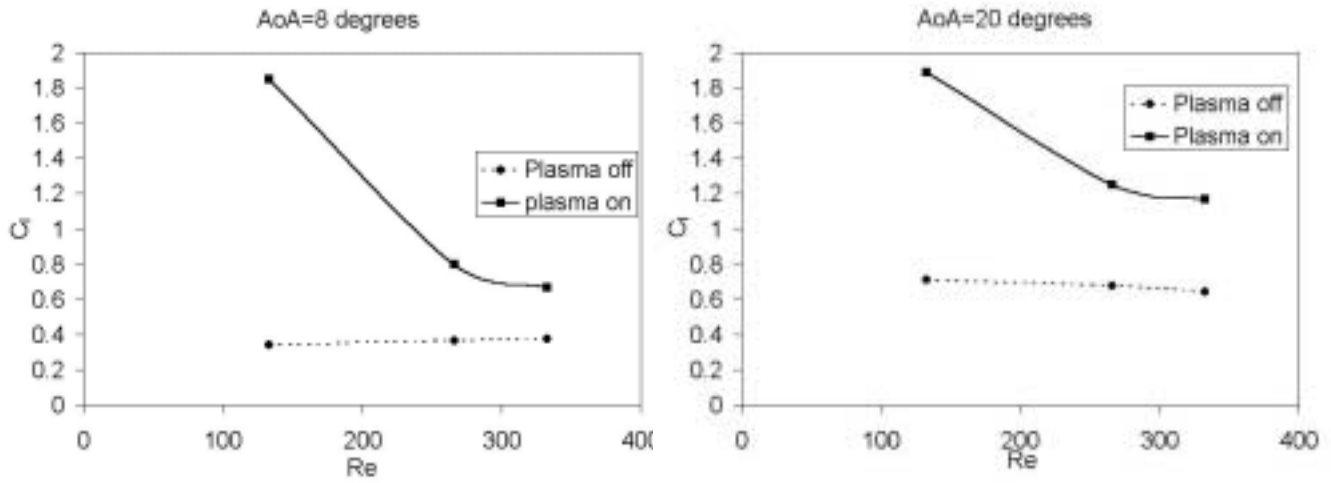


(b) Re=266



(c) Re=333

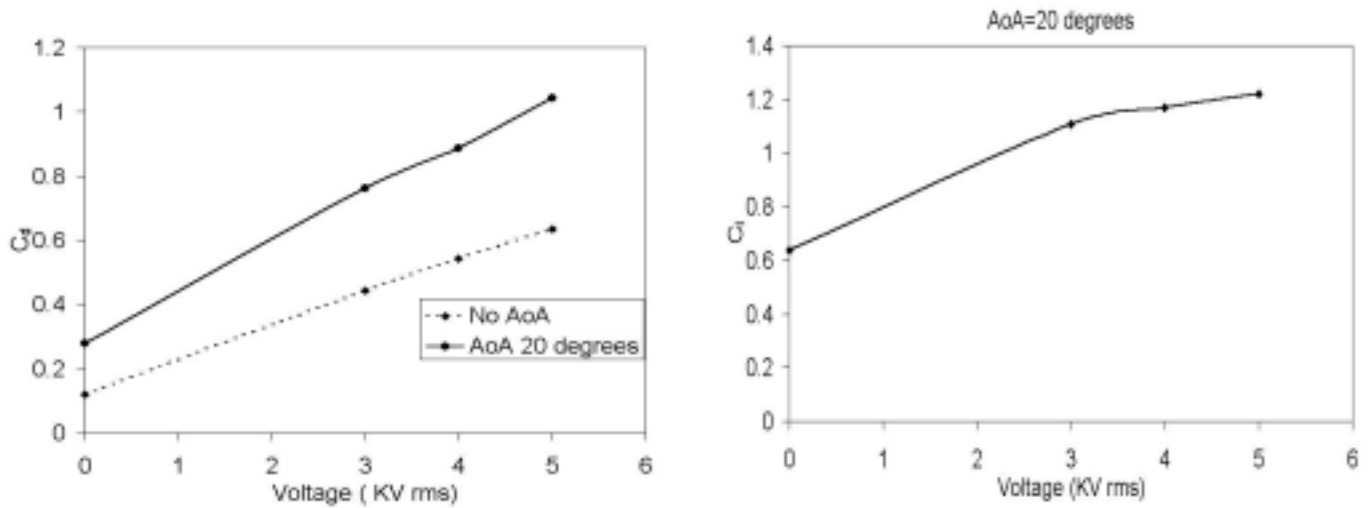
Figure 5. Drag variation with angle of attack for various Re. The plasma is operated at 4KV rms and 3KHz.



(a) Angle of attack= 8 degrees

(b) Angle of attack =20 degrees

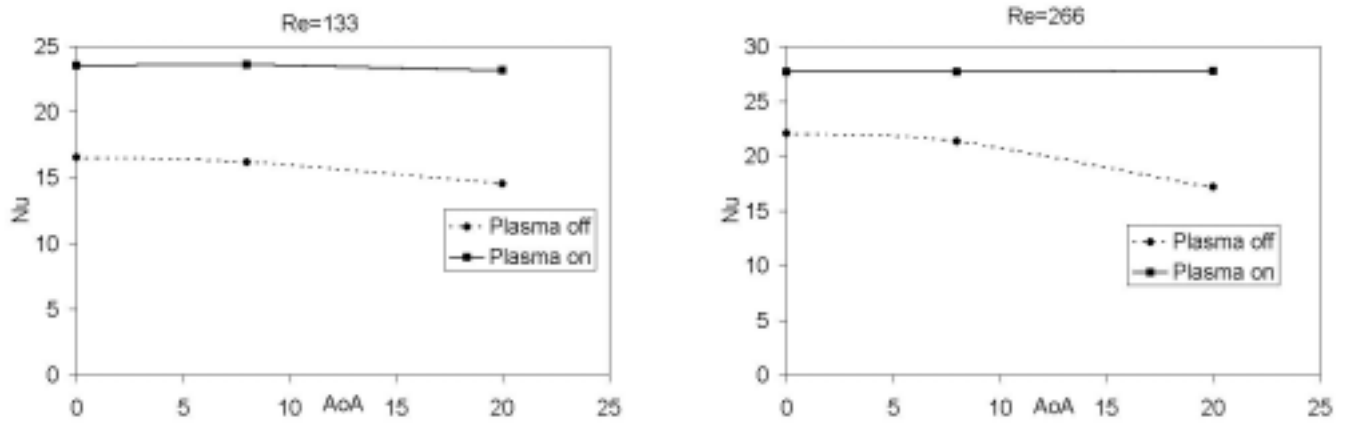
Figure 6. Variation of lift with Re for different angles of attack. The plasma is operated at 4KV rms and 3KHz.



(a) Effect of voltage on drag for $Re=333$ different angles of attack

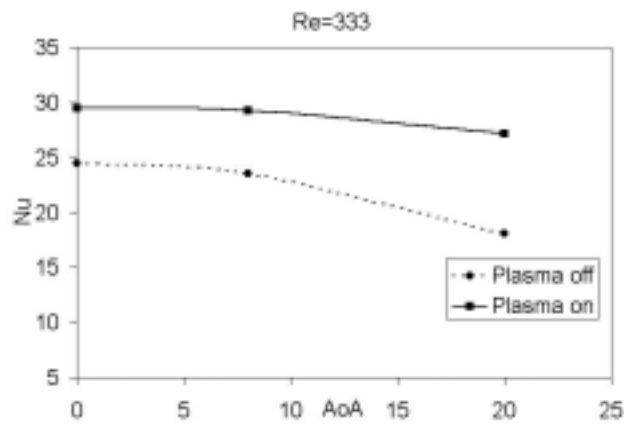
(b) Effect of voltage on lift at $Re=333$ and angle of attack of twenty degrees.

Figure 7. Effect of voltage on aerodynamics at $Re=333$



(a) Re=133

(b) Re=266



(c) Re=333

Figure 8. Nusselt number variation with angle of attack for various Reynolds number. The plasma is operated at 4KV rms and 3KHz frequency.

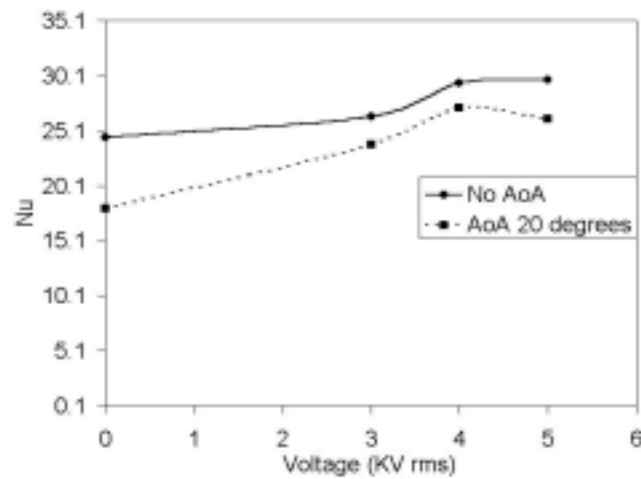
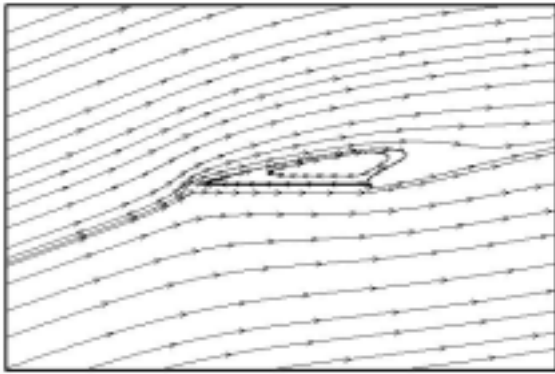
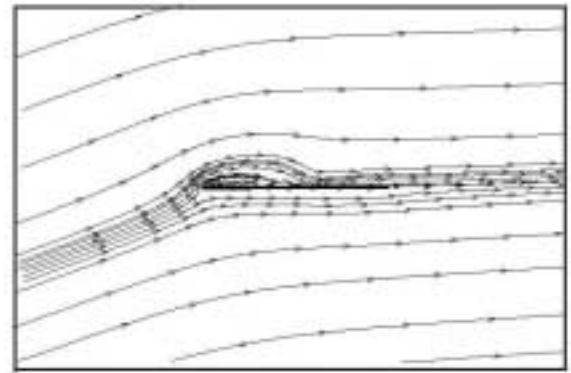


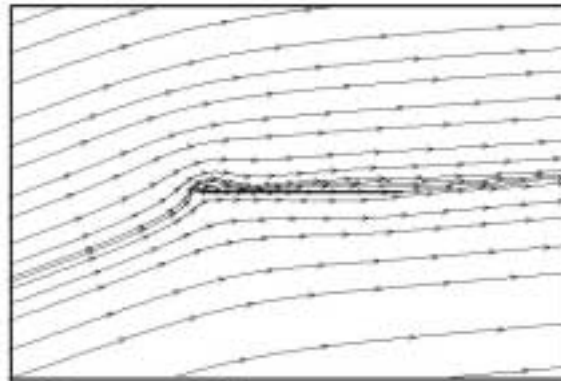
Figure 9. Dependence of the heat transfer on the applied voltage for Re=333 and two different angles of attack.



(a) Plasma off



(b) Plasma on with electrode at 0.51.



(c) Plasma on with electrode placed at 0.11 from the leading edge.

Figure 10. Streamlines showing flow separation for $Re=333$ and an angle of attack twenty degrees for different positions of the electrode.